Frequency Domain Filters

Andrea Torsello
DAIS
Università Ca' Foscari
via Torino 155,
30172 Mestre (VE)

Fourier Theorem

UNIVERSITÀ
CA' FOSCARI
VENEZIA

Fourier Theorem: every square integrable periodic function can be approximated arbitrarily well with a series of trigonometric functions

$$S_m(f) = \sum_{v=-m}^{m} \left[a_v \cos(\omega v x) + b_v \sin(\omega v x) \right]$$

$$\lim_{m \to \infty} \|f - S_m(f)\|^2 = 0$$

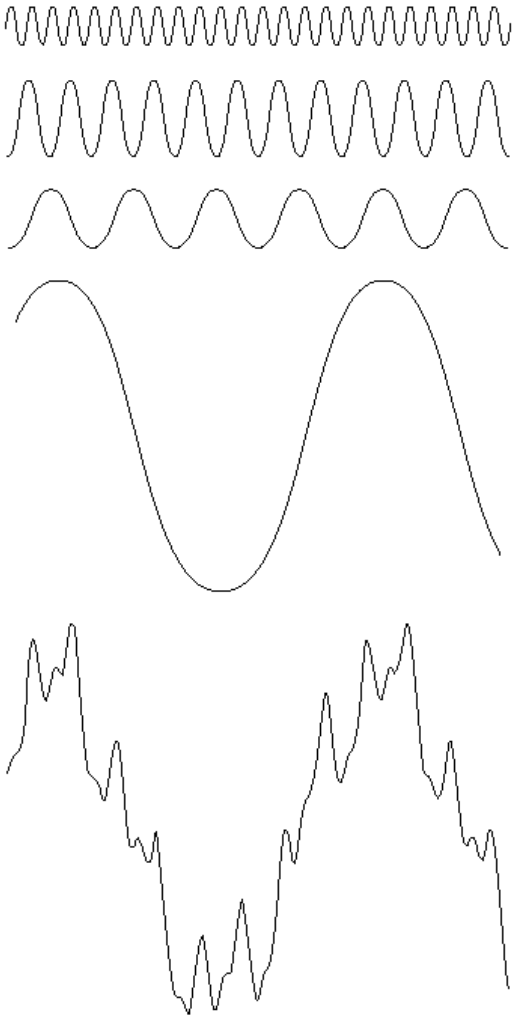

FIGURE 4.1 The function at the bottom is the sum of the four functions above it. Fourier's idea in 1807 that periodic functions could be represented as a weighted sum of sines and cosines was met with skepticism.

Fourier Transform of an image

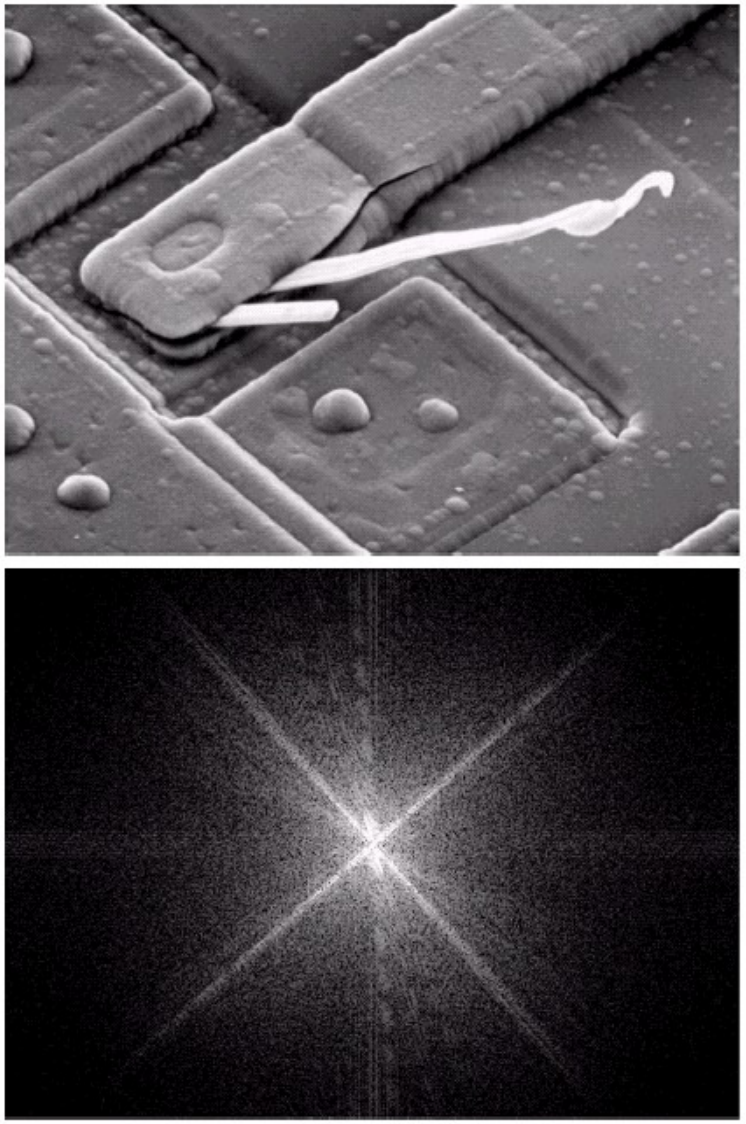

a
b

FIGURE 4.4
(a) SEM image of a damaged integrated circuit. (b) Fourier spectrum of (a). (Original image courtesy of Dr. J. M. Hudak, Brockhouse Institute for Materials Research, McMaster University, Hamilton, Ontario, Canada.)

Shift

- Normally 0 is at the corners, for clarity we will shift it to the center

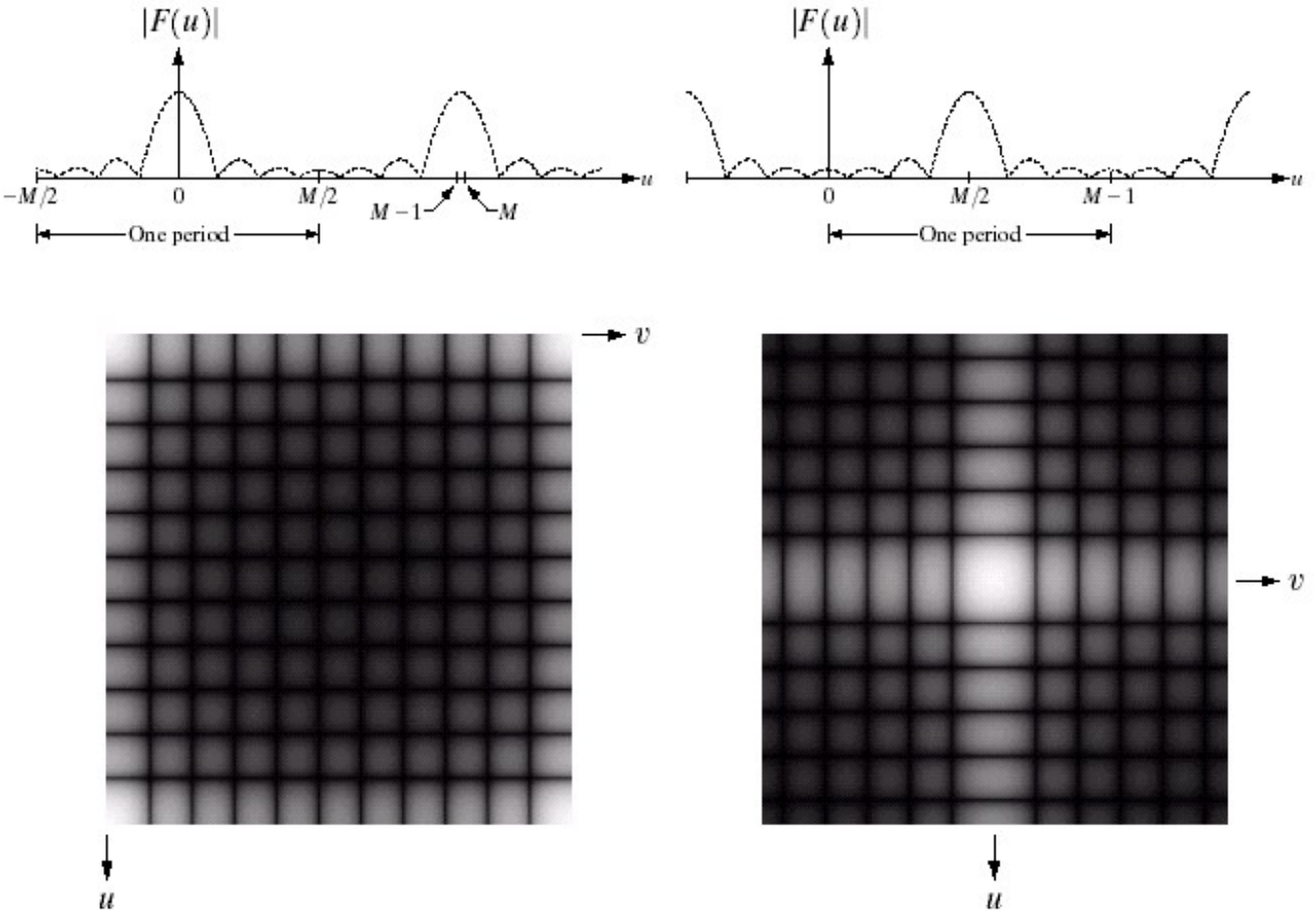

a b
c d

FIGURE 4.34
(a) Fourier spectrum showing back-to-back half periods in the interval $[0, M-1]$. (b) Shifted spectrum showing a full period in the same interval. (c) Fourier spectrum of an image, showing the same back-to-back properties as (a), but in two dimensions. (d) Centered Fourier spectrum.

Low-pass filter

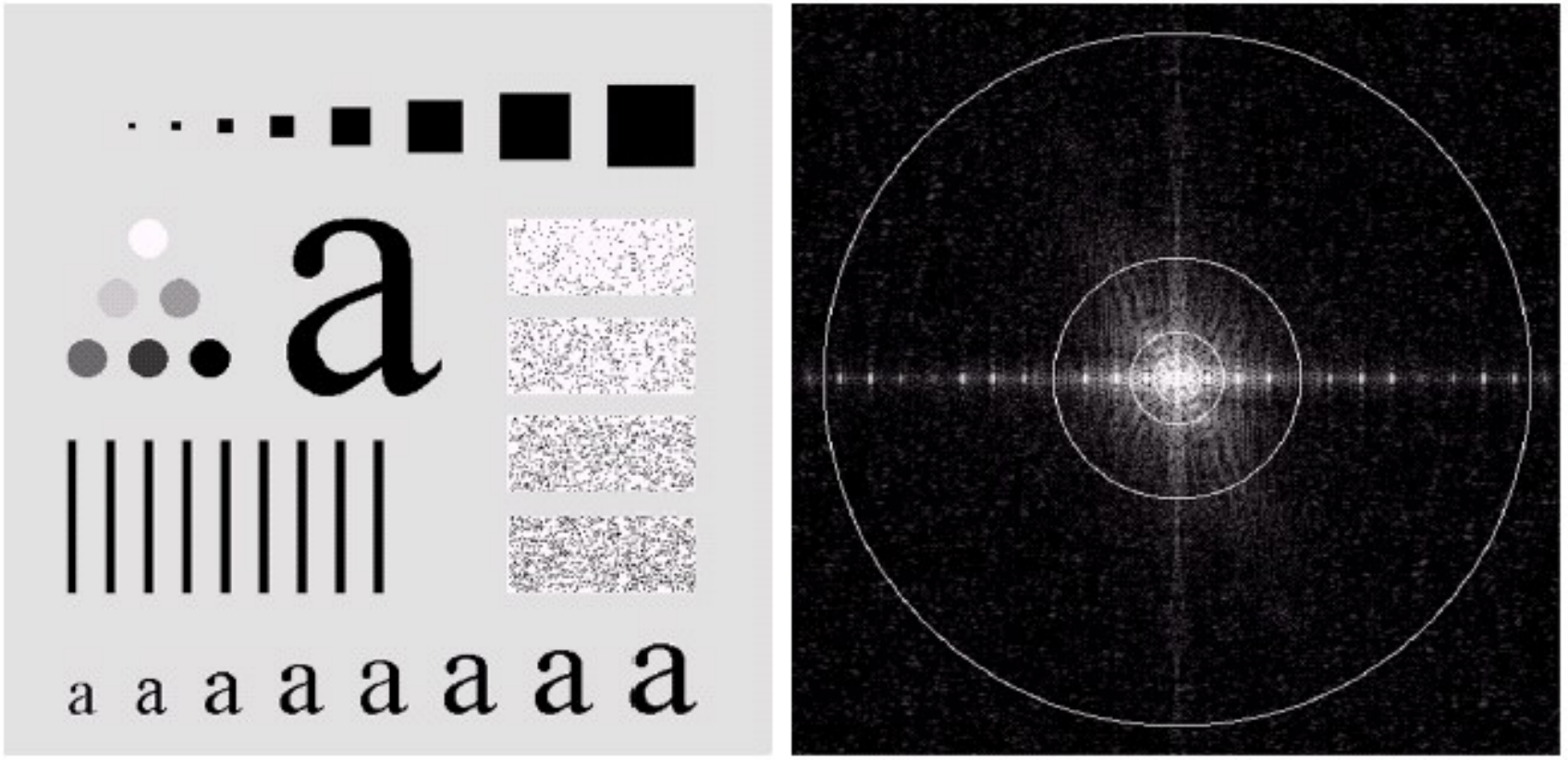

a b

FIGURE 4.11 (a) An image of size 500 × 500 pixels and (b) its Fourier spectrum. The superimposed circles have radii values of 5, 15, 30, 80, and 230, which enclose 92.0, 94.6, 96.4, 98.0, and 99.5% of the image power, respectively.

Ideal low-pass filter

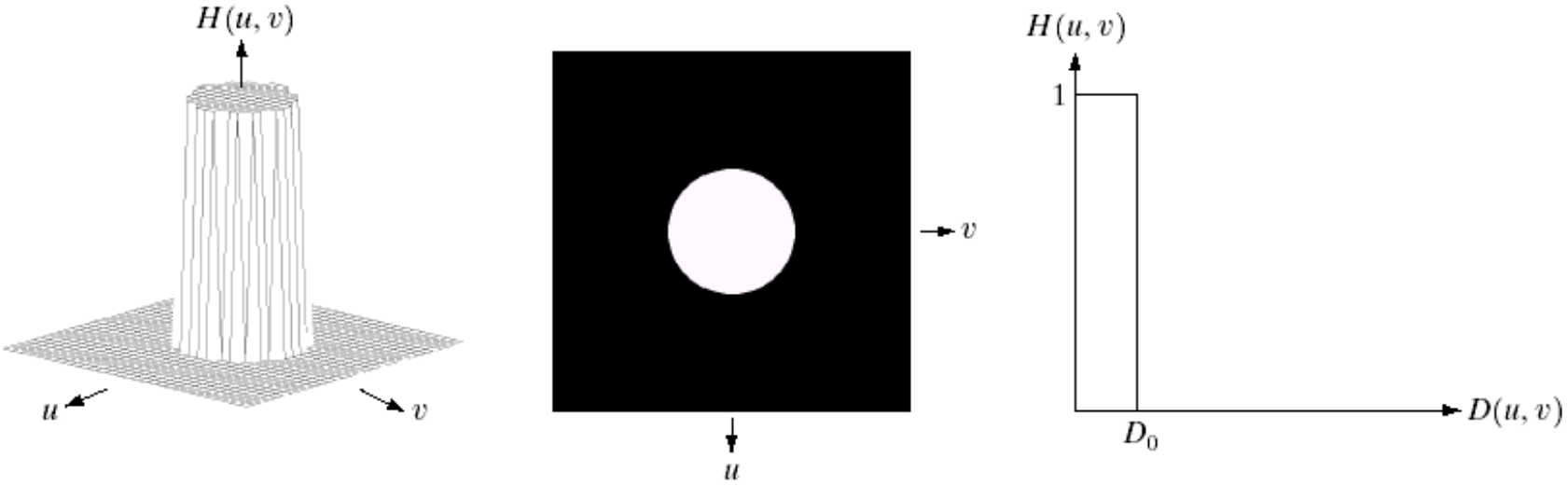

a b c

FIGURE 4.10 (a) Perspective plot of an ideal lowpass filter transfer function. (b) Filter displayed as an image. (c) Filter radial cross section.

Ringing

UNIVERSITÀ CA' FOSCARI VENEZIA

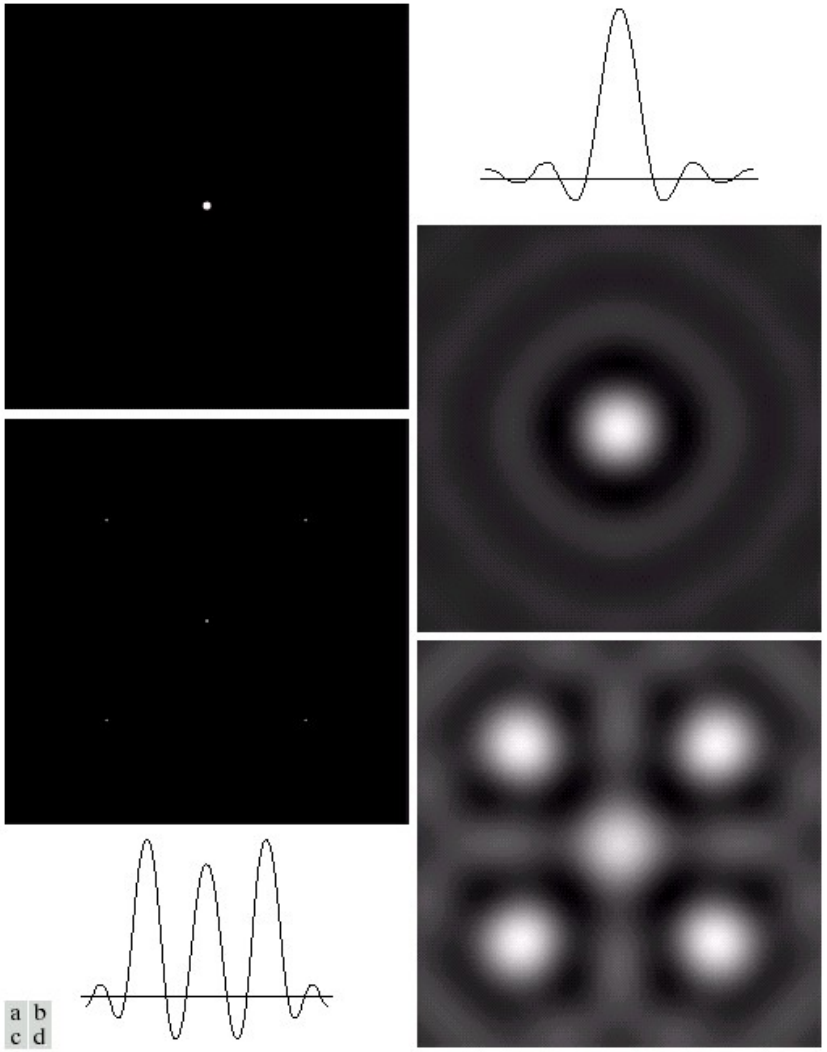

a b
c d

FIGURE 4.13 (a) A frequency-domain ILPF of radius 5. (b) Corresponding spatial filter (note the ringing). (c) Five impulses in the spatial domain, simulating the values of five pixels. (d) Convolution of (b) and (c) in the spatial domain.

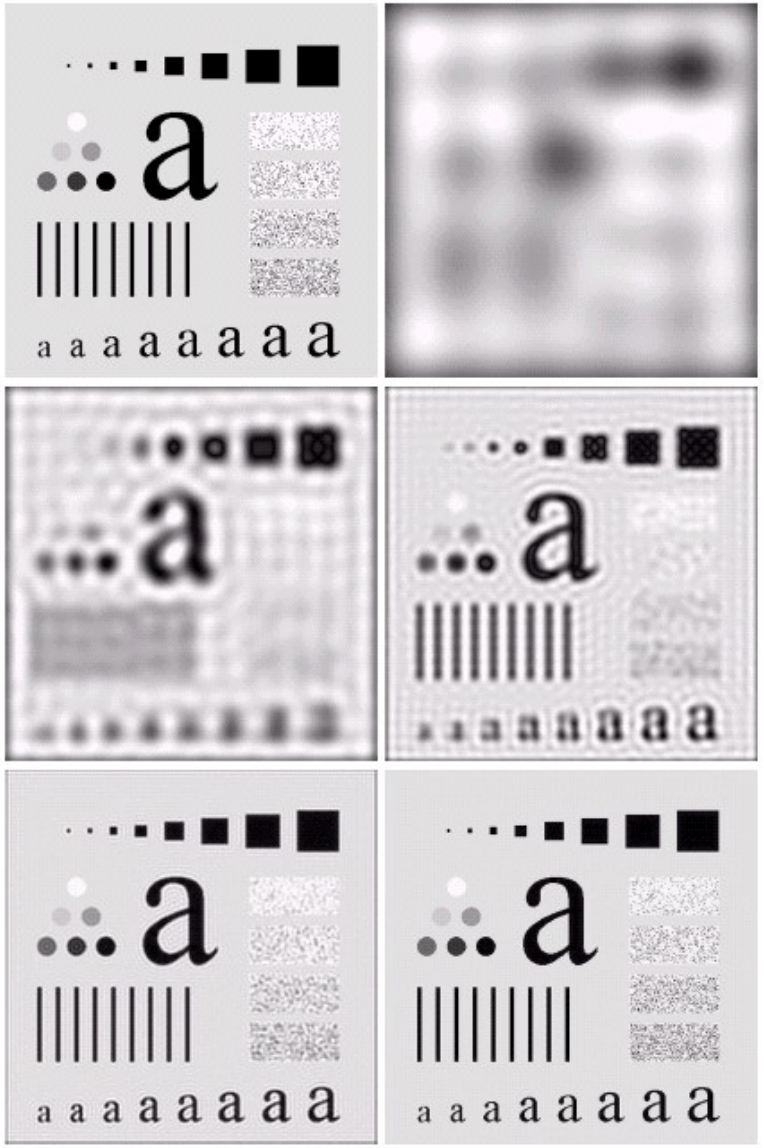

Transform of a box function

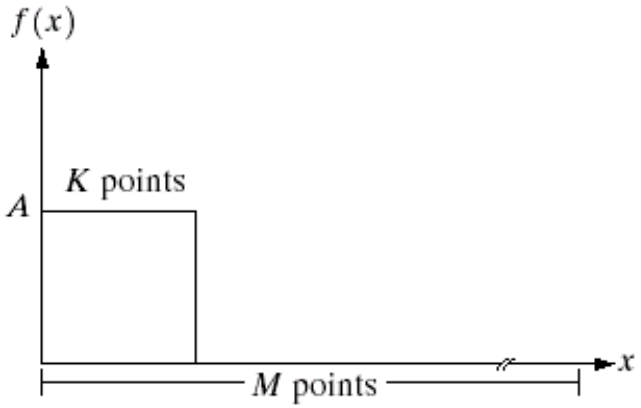

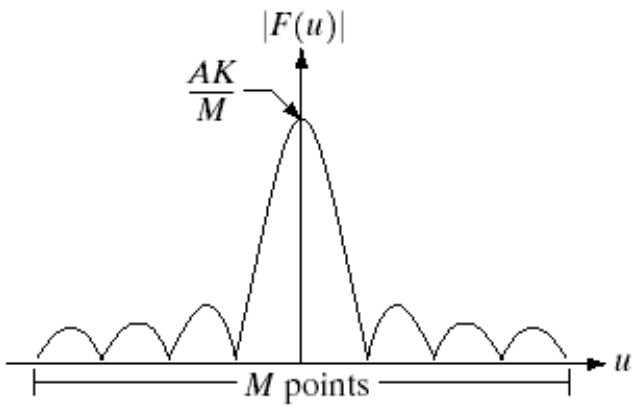

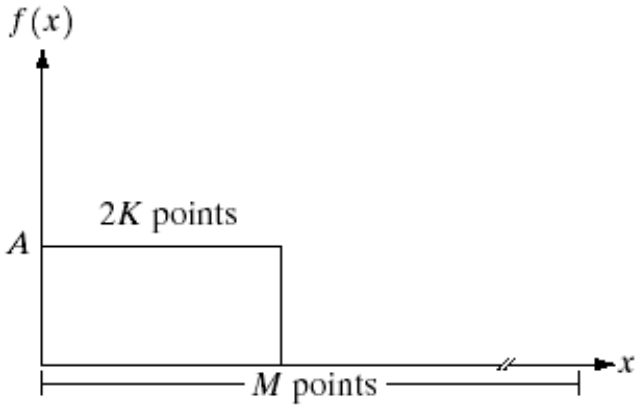

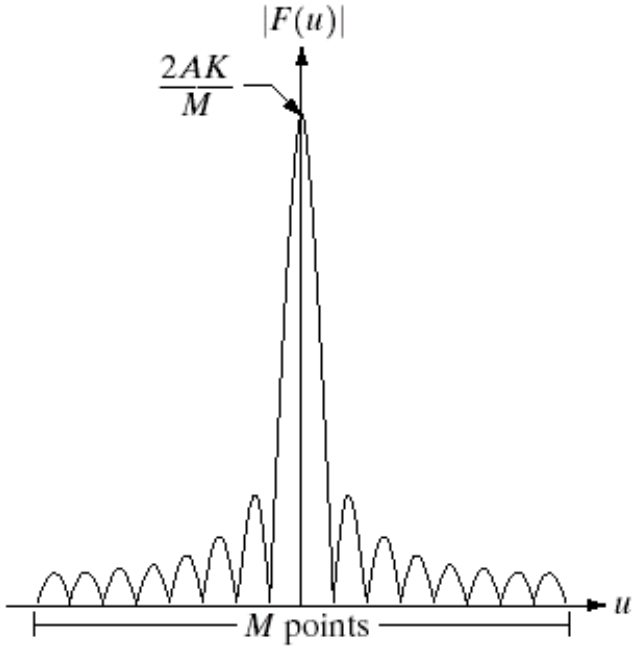

a b
c d

FIGURE 4.2 (a) A discrete function of M points, and (b) its Fourier spectrum. (c) A discrete function with twice the number of nonzero points, and (d) its Fourier spectrum.

Transform of the average filter

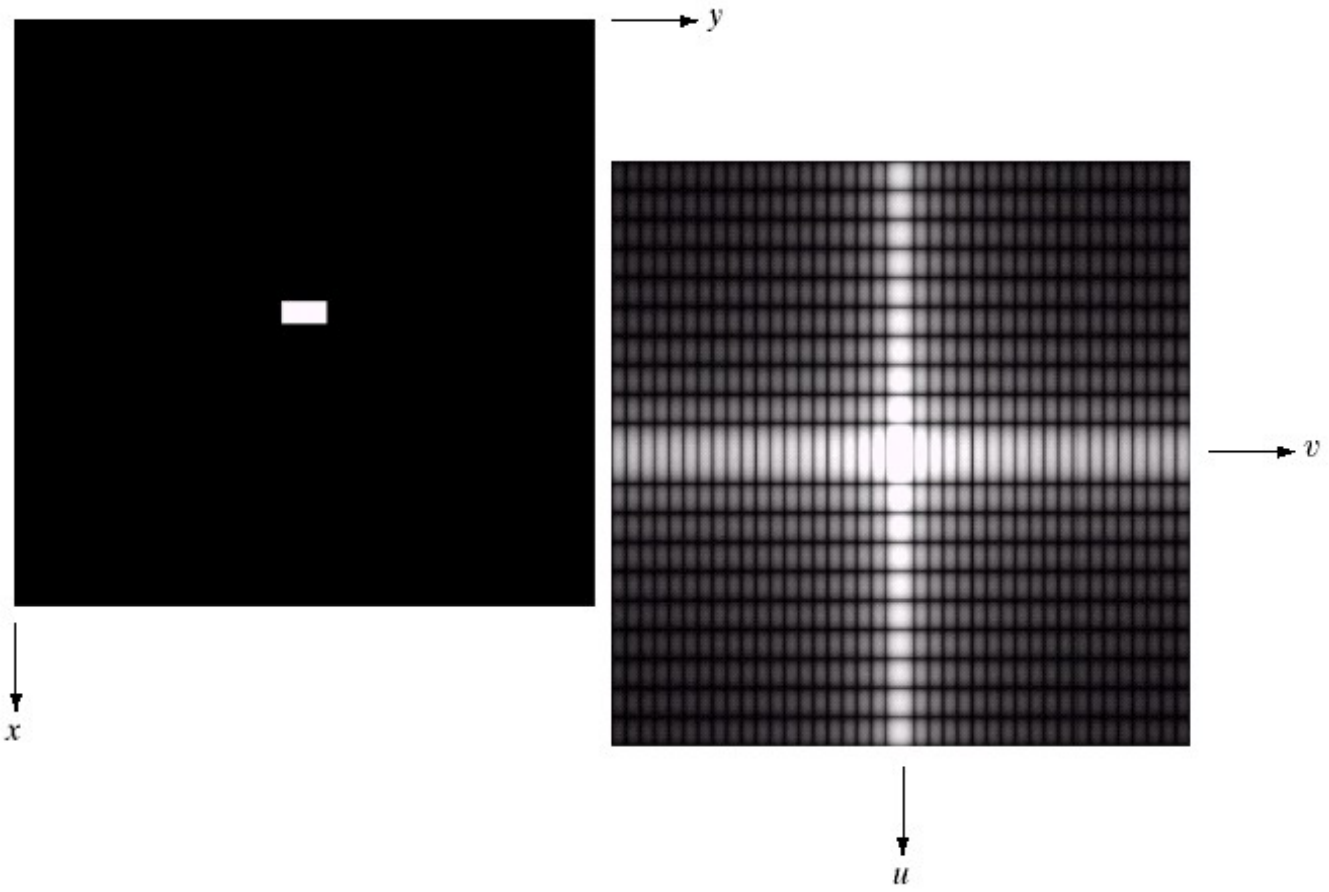

a b

FIGURE 4.3
(a) Image of a 20×40 white rectangle on a black background of size 512×512 pixels.
(b) Centered Fourier spectrum shown after application of the log transformation given in Eq. (3.2-2). Compare with Fig. 4.2.

Butterworth filter

UNIVERSITÀ CA' FOSCARI VENEZIA

$$H(u,v)=\frac{1}{1+\left[D(u,v)/D_0\right]^{2n}}$$

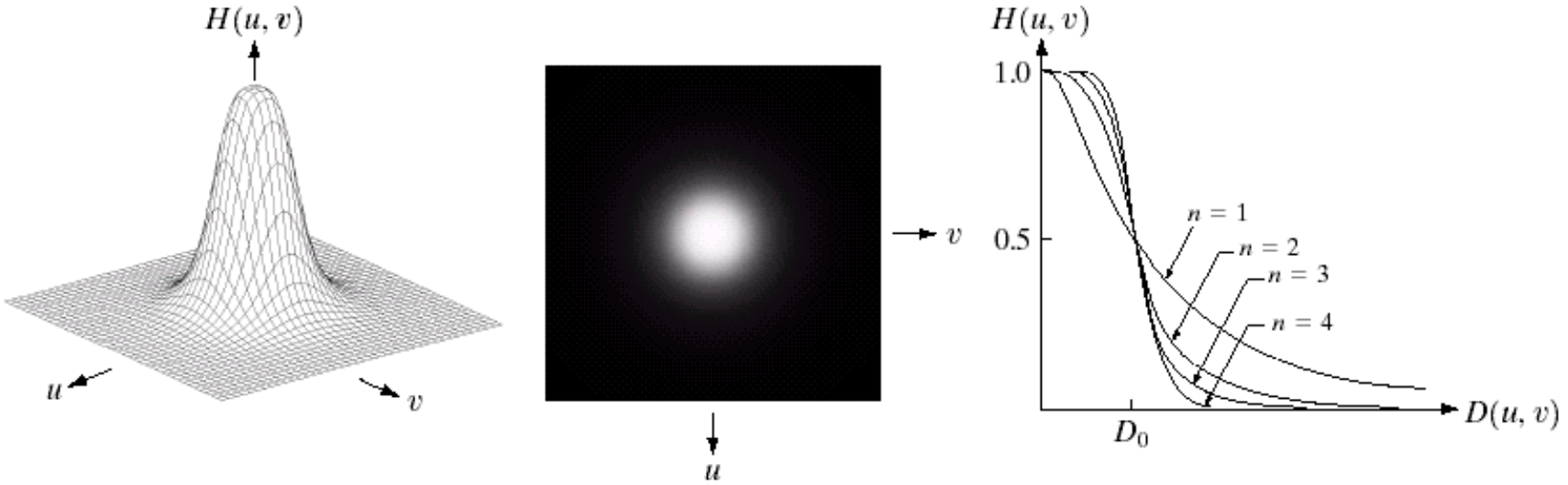

a b c

FIGURE 4.14 (a) Perspective plot of a Butterworth lowpass filter transfer function. (b) Filter displayed as an image. (c) Filter radial cross sections of orders 1 through 4.

Butterworth filter

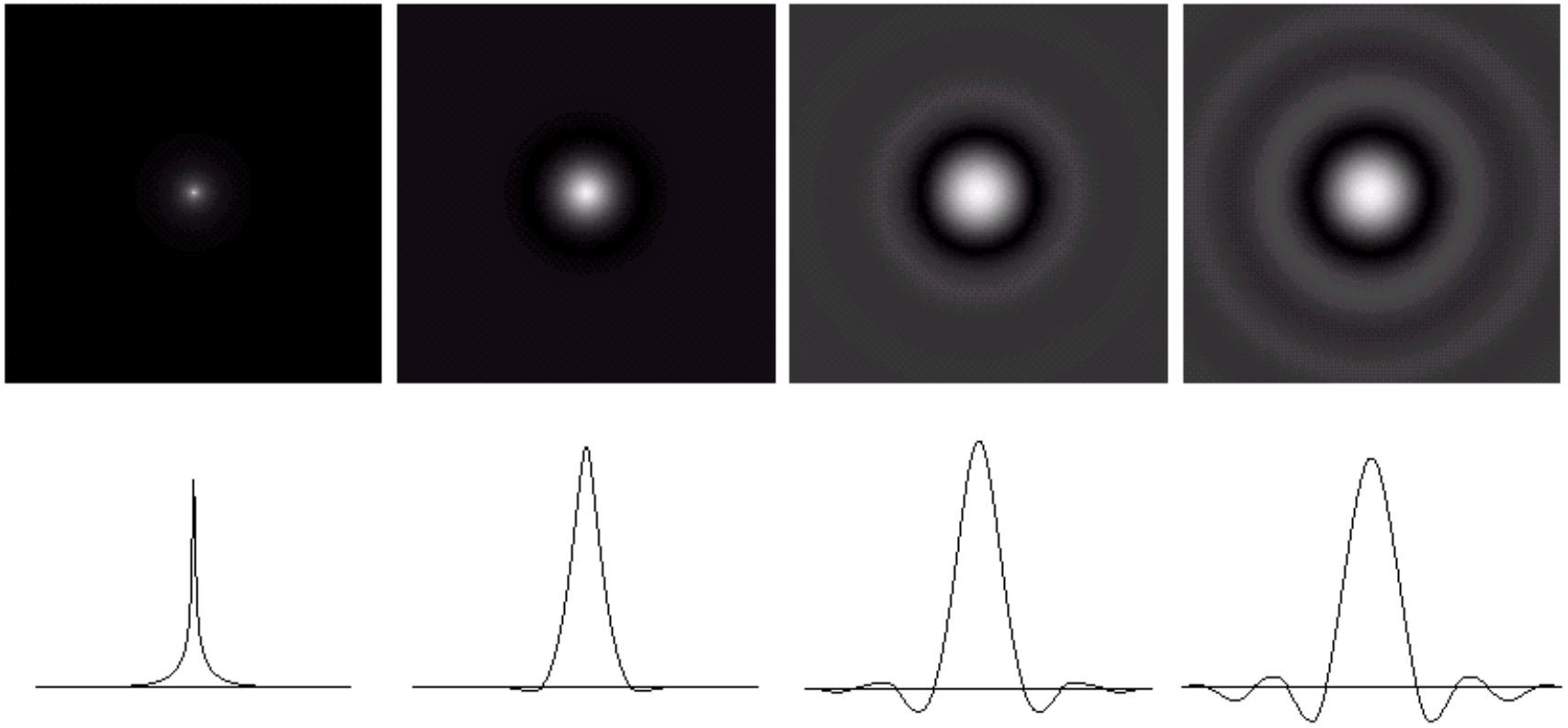

a b c d

FIGURE 4.16 (a)–(d) Spatial representation of BLPFs of order 1, 2, 5, and 20, and corresponding gray-level profiles through the center of the filters (all filters have a cutoff frequency of 5). Note that ringing increases as a function of filter order.

Butterworth filter

Ringing is significantly reduced

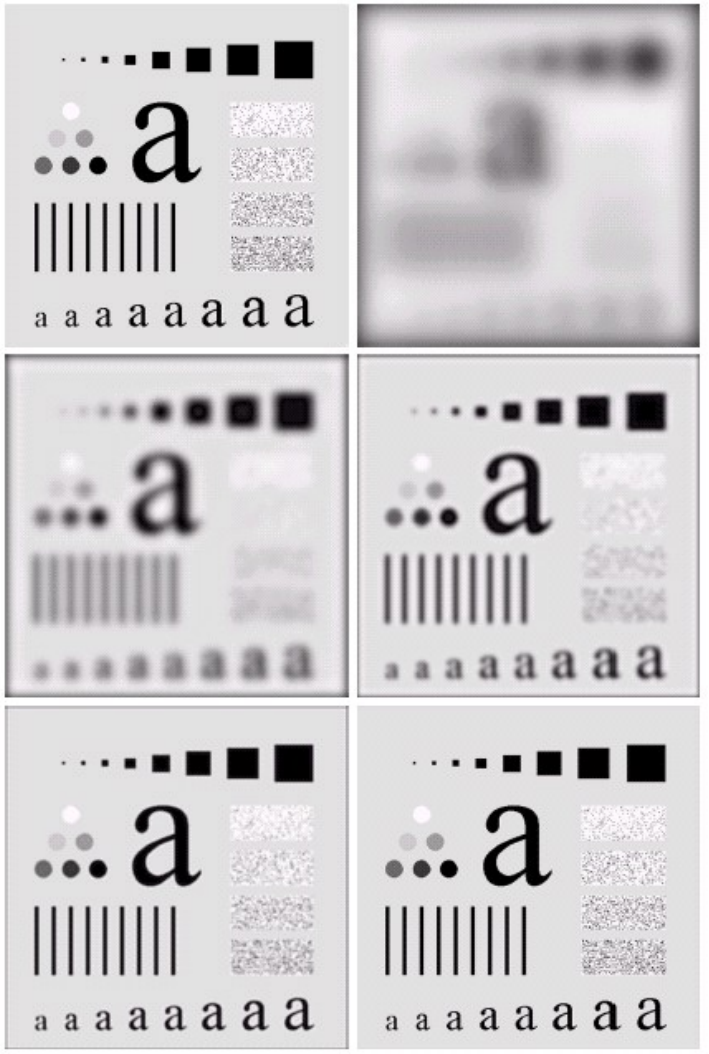

a b
c d
e f

FIGURE 4.15 (a) Original image. (b)–(f) Results of filtering with BLPFs of order 2, with cutoff frequencies at radii of 5, 15, 30, 80, and 230, as shown in Fig. 4.11(b). Compare with Fig. 4.12.

Gaussian filter

UNIVERSITÀ CA' FOSCARI VENEZIA

$$H(u,v) = \frac{1}{\sqrt{2\pi}\,D_0} e^{-\frac{1}{2}\left(\frac{D(u,v)}{D_0}\right)^2}$$

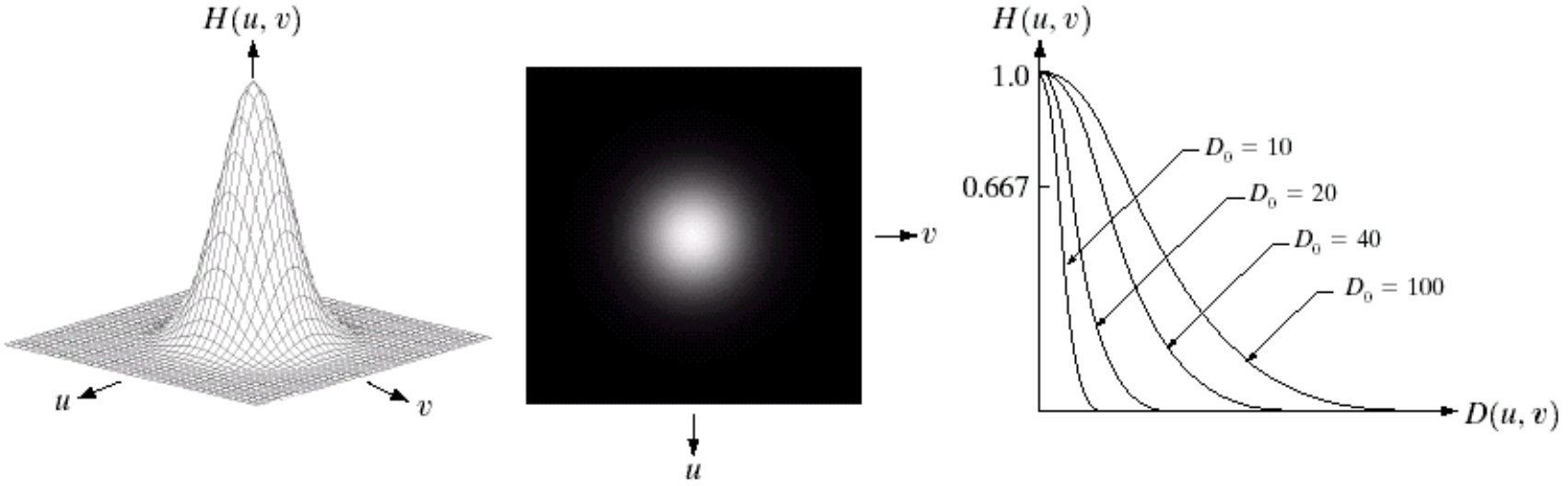

a b c

FIGURE 4.17 (a) Perspective plot of a GLPF transfer function. (b) Filter displayed as an image. (c) Filter radial cross sections for various values of D_0.

Gaussian filter

There is no ringing

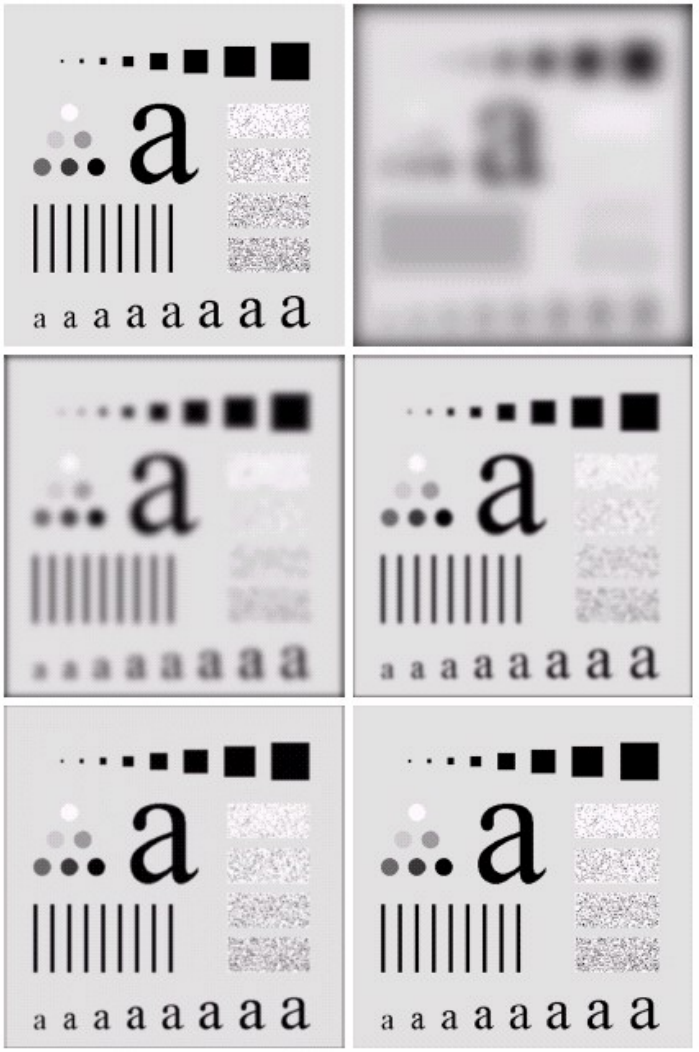

FIGURE 4.18 (a) Original image. (b)–(f) Results of filtering with Gaussian lowpass filters with cutoff frequencies set at radii values of 5, 15, 30, 80, and 230, as shown in Fig. 4.11(b). Compare with Figs. 4.12 and 4.15.

Gaussian filter

a b c

FIGURE 4.20 (a) Original image (1028 × 732 pixels). (b) Result of filtering with a GLPF with $D_0 = 100$. (c) Result of filtering with a GLPF with $D_0 = 80$. Note reduction in skin fine lines in the magnified sections of (b) and (c).

Gaussian filter

a b c

FIGURE 4.21 (a) Image showing prominent scan lines. (b) Result of using a GLPF with $D_0 = 30$. (c) Result of using a GLPF with $D_0 = 10$. (Original image courtesy of NOAA.)

High-pass filter

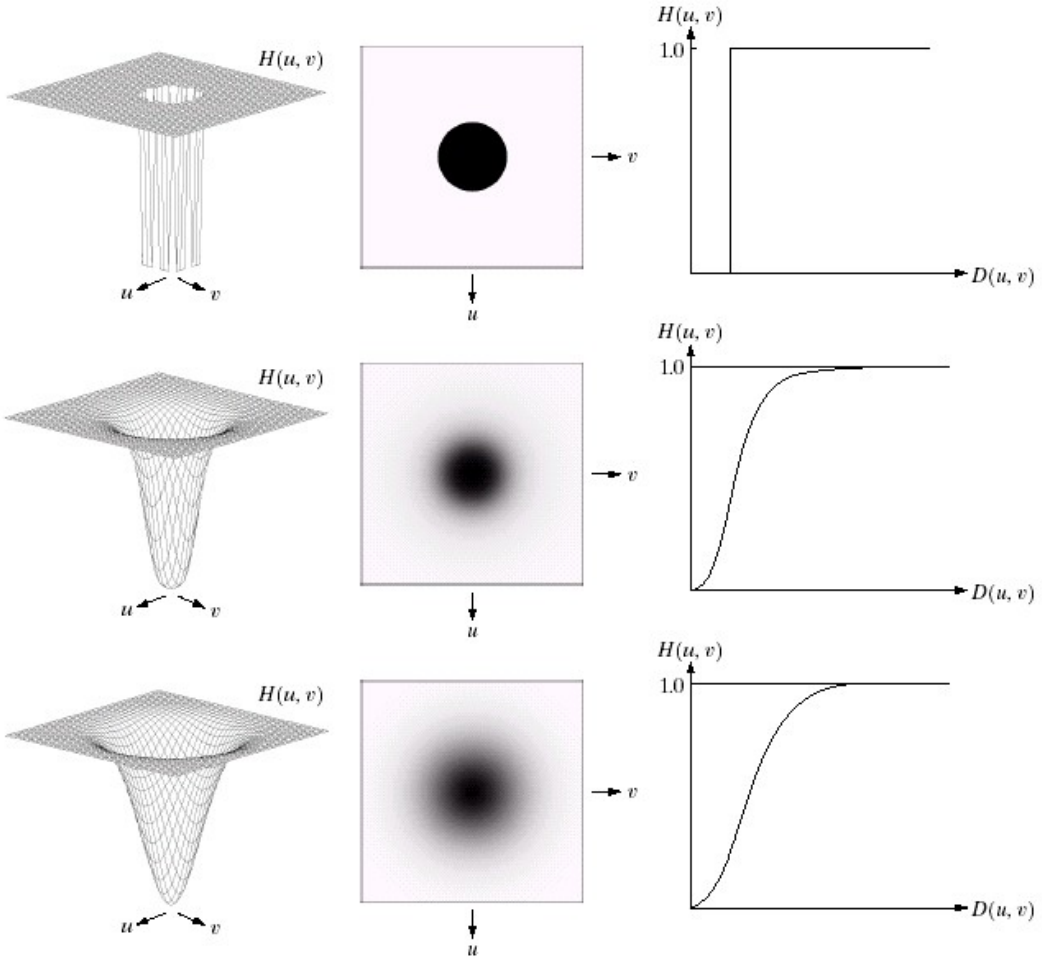

a b c
d e f
g h i

FIGURE 4.22 Top row: Perspective plot, image representation, and cross section of a typical ideal highpass filter. Middle and bottom rows: The same sequence for typical Butterworth and Gaussian highpass filters.

UNIVERSITÀ
CA' FOSCARI
VENEZIA

High-pass filter

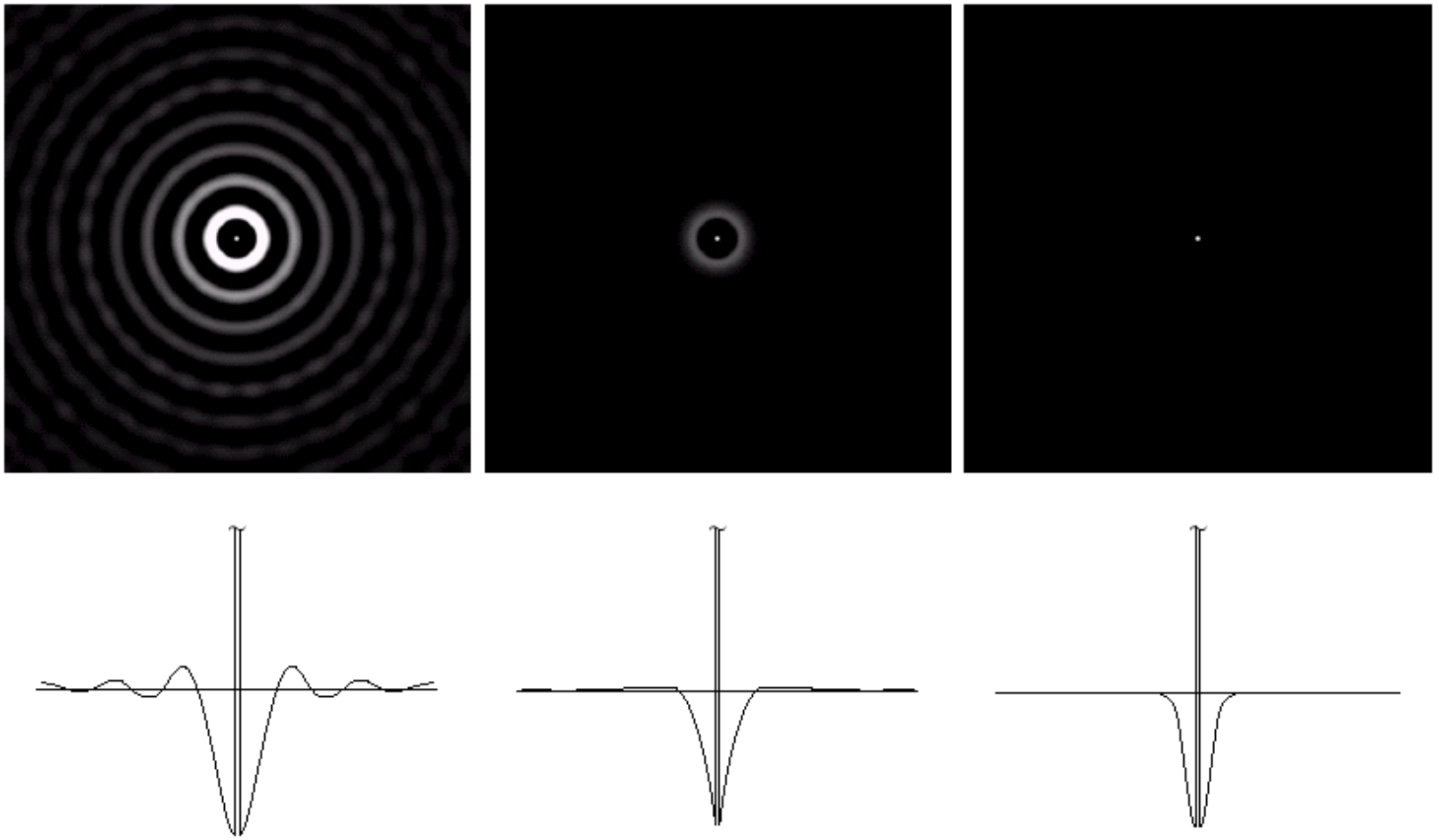

a b c

FIGURE 4.23 Spatial representations of typical (a) ideal, (b) Butterworth, and (c) Gaussian frequency domain highpass filters, and corresponding gray-level profiles.

Ideal High-pass filter

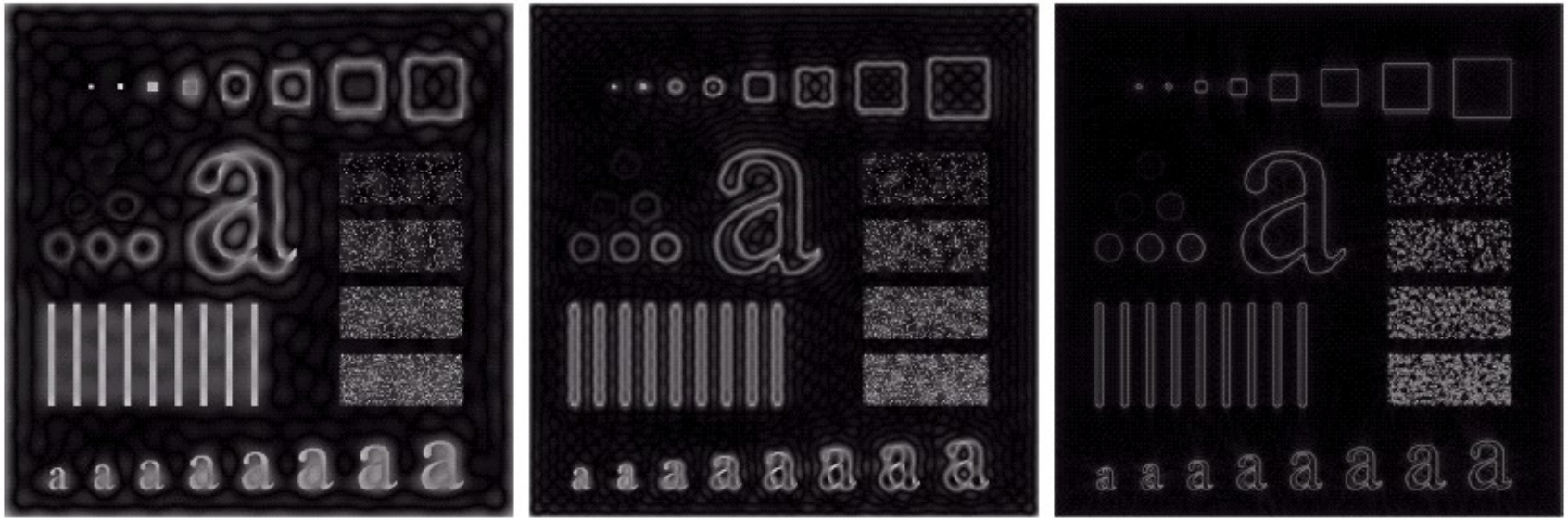

a b c

FIGURE 4.24 Results of ideal highpass filtering the image in Fig. 4.11(a) with $D_0 = 15$, 30, and 80, respectively. Problems with ringing are quite evident in (a) and (b).

Butterworth High-pass filter

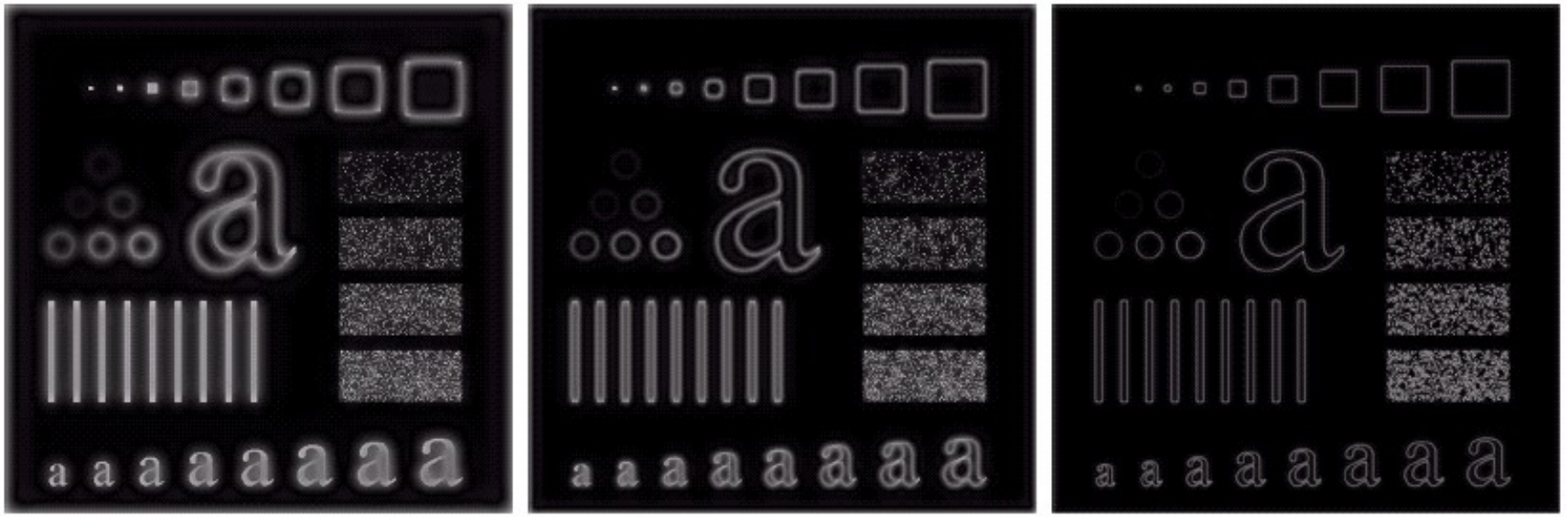

a b c

FIGURE 4.25 Results of highpass filtering the image in Fig. 4.11(a) using a BHPF of order 2 with $D_0 = 15$, 30, and 80, respectively. These results are much smoother than those obtained with an ILPF.

Gaussiano High-pass filter

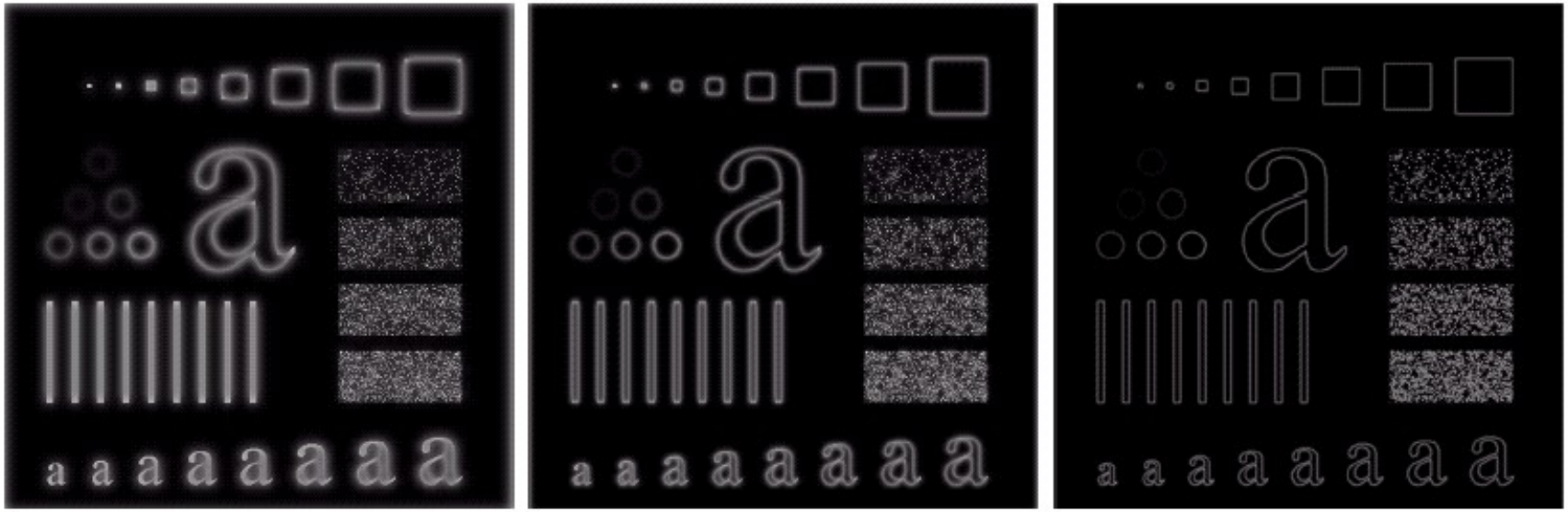

a b c

FIGURE 4.26 Results of highpass filtering the image of Fig. 4.11(a) using a GHPF of order 2 with $D_0 = 15$, 30, and 80, respectively. Compare with Figs. 4.24 and 4.25.

Correlation

UNIVERSITÀ CA' FOSCARI VENEZIA

$$(f \circ g)(x,y) = \frac{1}{MN} \sum_{m=0}^{M-1} \sum_{n=0}^{N-1} \overline{f(m,n)}\, h(x+m, y+n)$$

$$F[f \circ g] = \overline{F(u,v)}\, H(u,v)$$

$$F[f \circ f] = |F(u,v)|^2$$

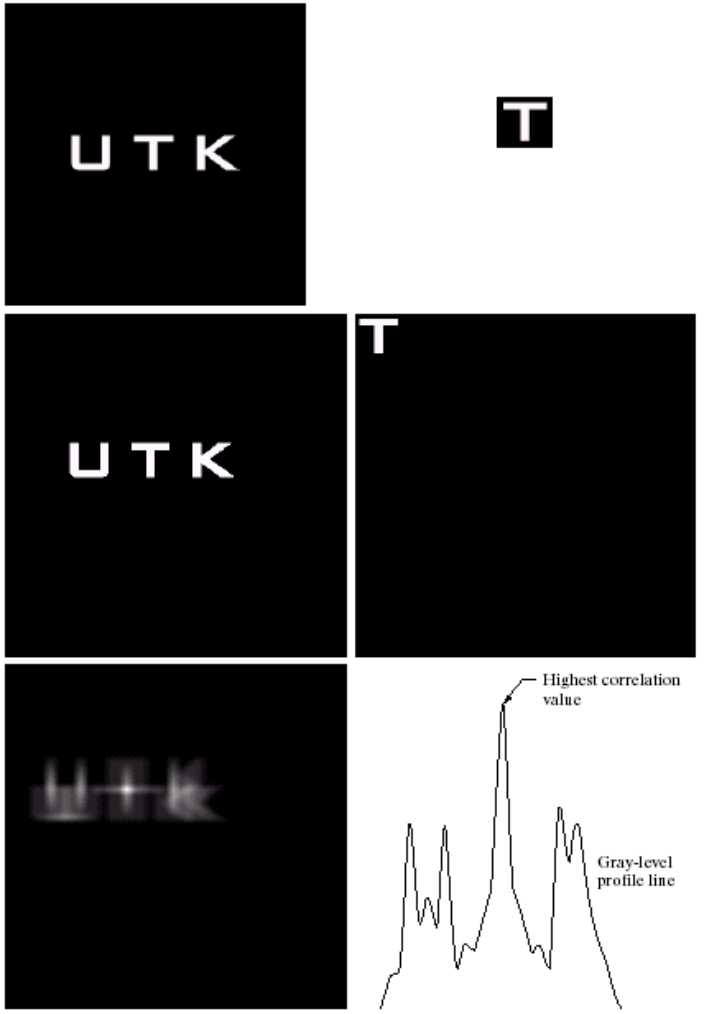

a b
c d
e f

FIGURE 4.41
(a) Image.
(b) Template.
(c) and
(d) Padded images.
(e) Correlation function displayed as an image.
(f) Horizontal profile line through the highest value in (e), showing the point at which the best match took place.

Notch filter

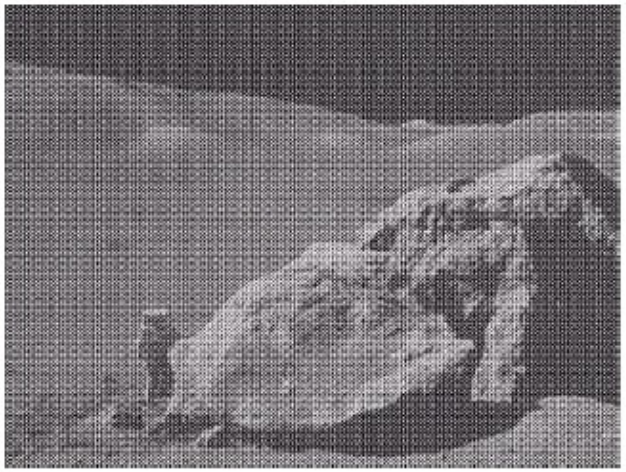

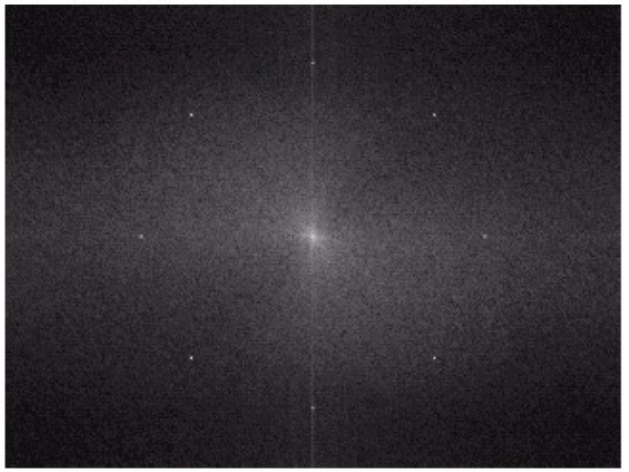

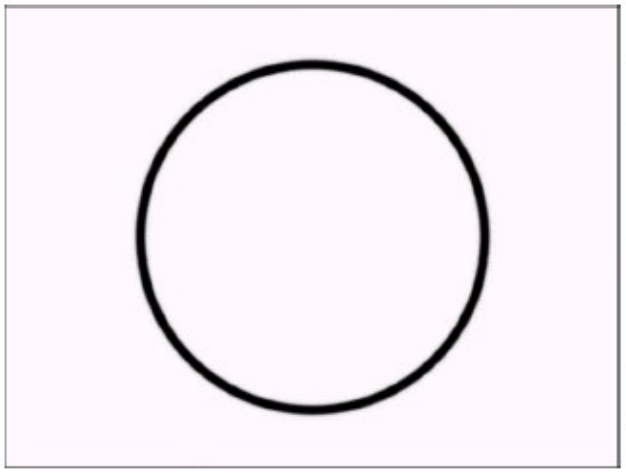

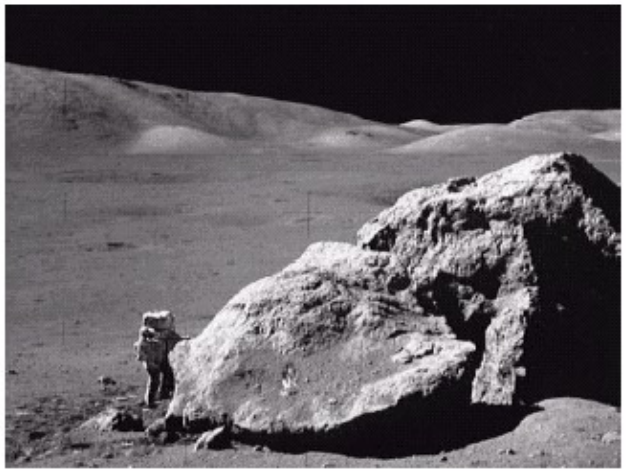

a b
c d

FIGURE 5.16
(a) Image corrupted by sinusoidal noise. (b) Spectrum of (a). (c) Butterworth bandreject filter (white represents 1). (d) Result of filtering. (Original image courtesy of NASA.)

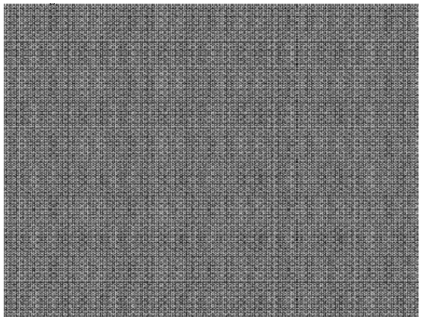

Notch filter

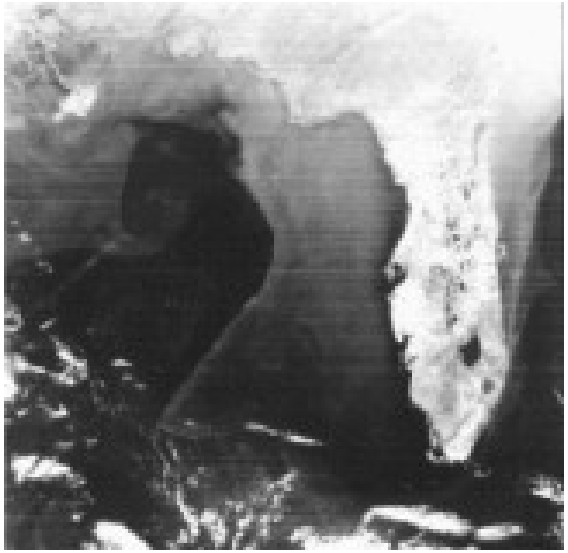

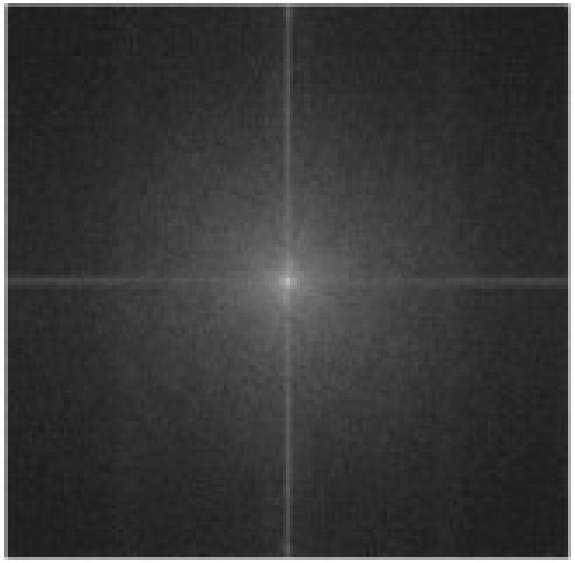

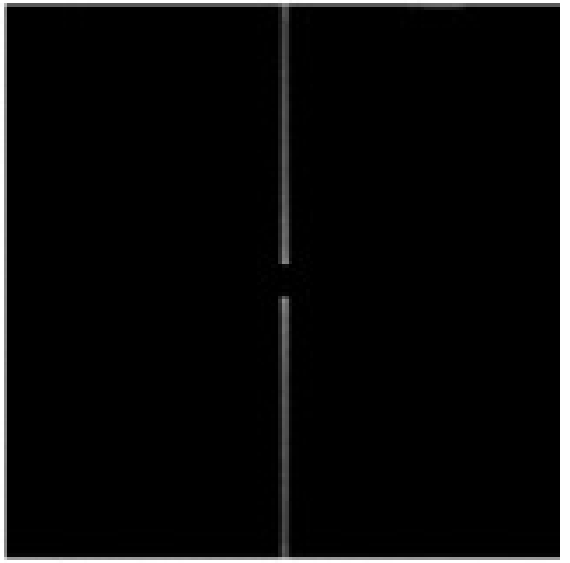

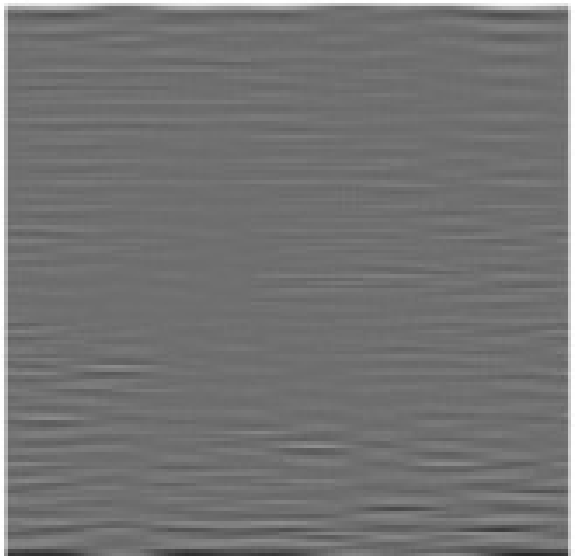

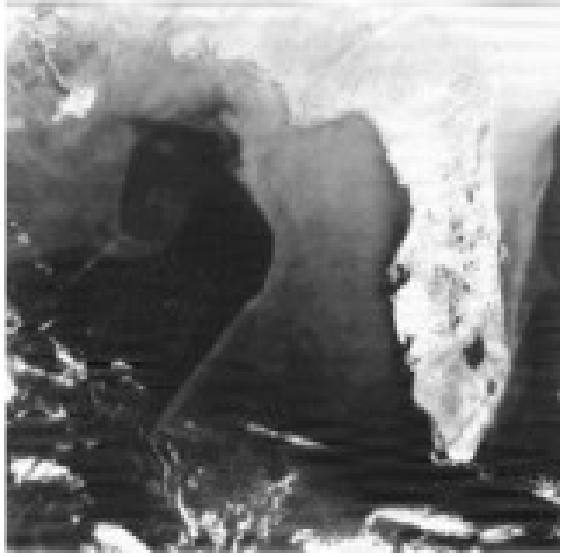

Analisys of periodic noise

a b

FIGURE 5.20
(a) Image of the Martian terrain taken by *Mariner 6.*
(b) Fourier spectrum showing periodic interference.
(Courtesy of NASA.)

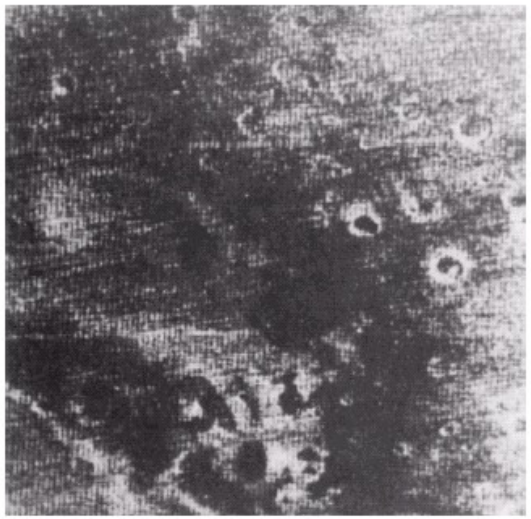

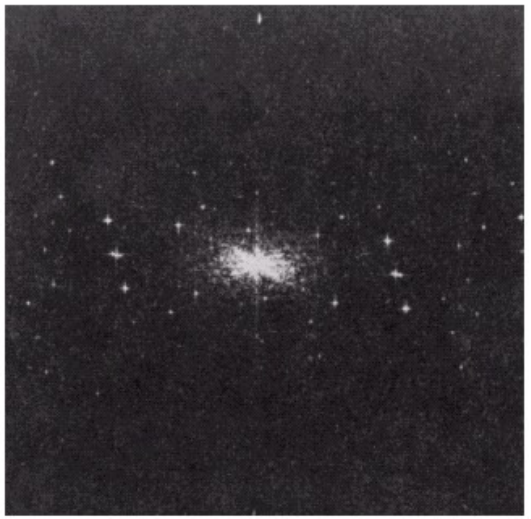

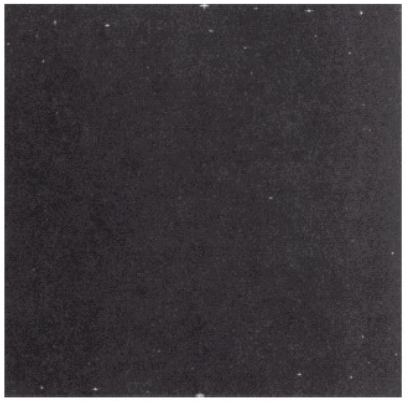

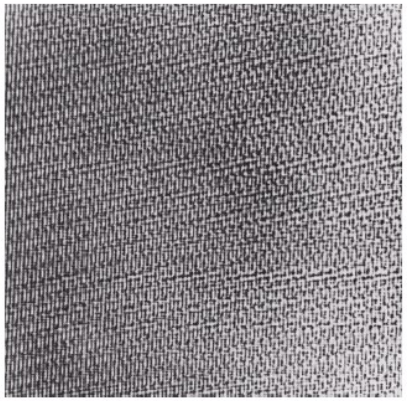

a b

FIGURE 5.22 (a) Fourier spectrum of $N(u, v)$, and (b) corresponding noise interference pattern $\eta(x, y)$. (Courtesy of NASA.)

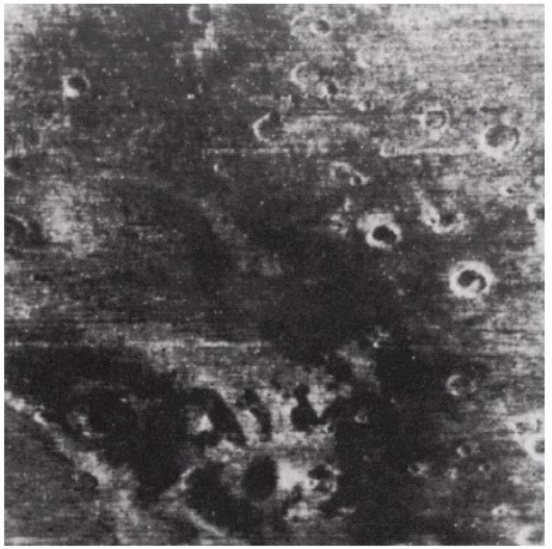

FIGURE 5.23 Processed image. (Courtesy of NASA.)

Homomorphic filter

$$I(x,y)=i(x,y)r(x,y)$$

$$z(x,y)=\ln I(x,y)=\ln i(x,y)+\ln r(x,y)$$

$$F[z(x,y)]=F[\ln i(x,y)]+F[\ln r(x,y)]$$

$$Z(u,v)=F_i(u,v)+F_r(u,v)$$

$$S(u,v)=Z(u,v)H(u,v)=F_i(u,v)H(u,v)+F_r(u,v)H(u,v)$$

$$s(x,y)=F^{-1}[S(u,v)]=i'(x,y)+r'(x,y)$$

$$i'(x,y)=F[F_i(u,v)H(u,v)]$$

$$r'(x,y)=F[F_r(u,v)H(u,v)]$$

$$g(x,y)=e^{s(x,y)}=e^{i'(x,y)}e^{r'(x,y)}=i_0(x,y)r_0(x,y)$$

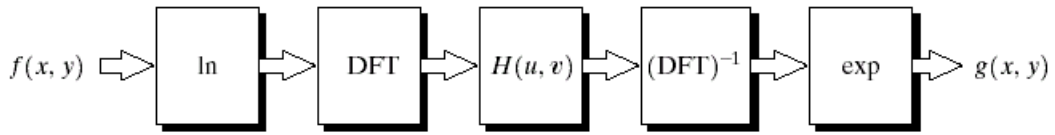

FIGURE 4.31 Homomorphic filtering approach for image enhancement.

Homomorphic filter

UNIVERSITÀ CA' FOSCARI VENEZIA

a b

FIGURE 4.33
(a) Original image. (b) Image processed by homomorphic filtering (note details inside shelter). (Stockham.)

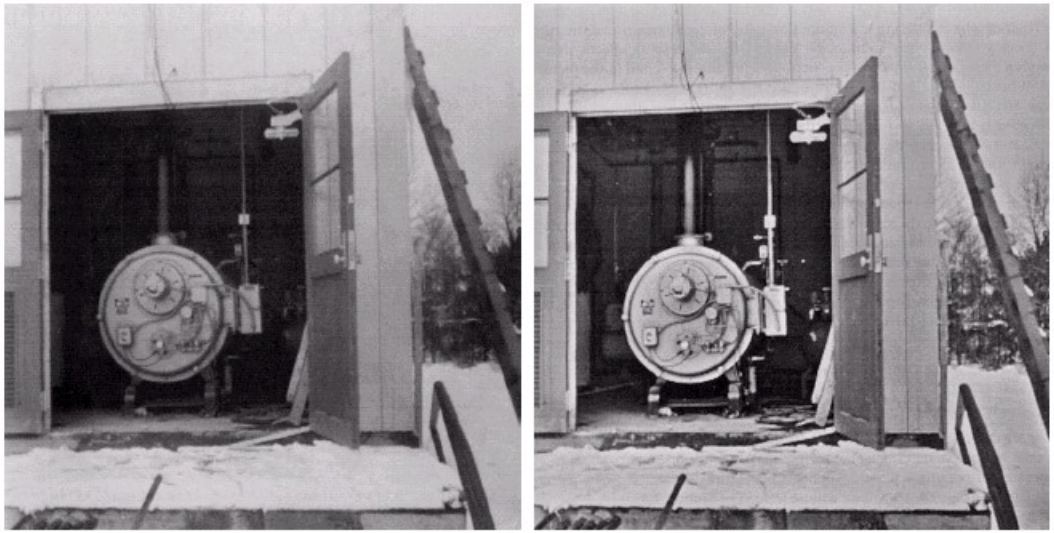

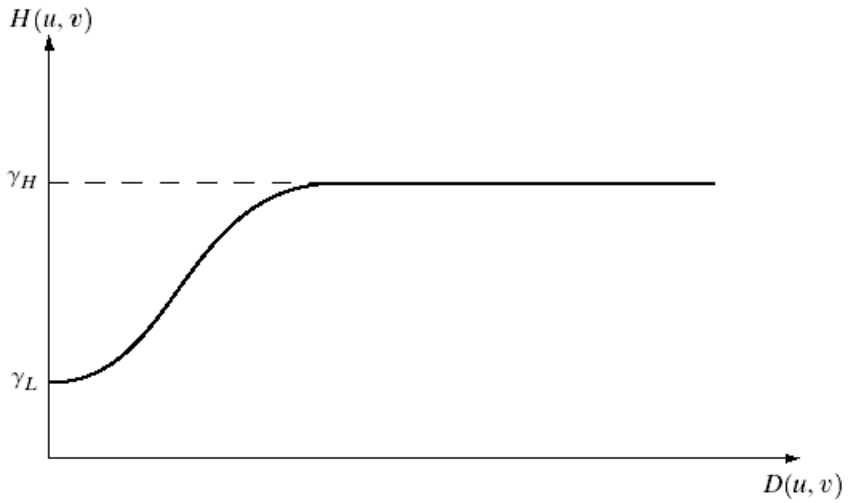

FIGURE 4.32
Cross section of a circularly symmetric filter function. $D(u, v)$ is the distance from the origin of the centered transform.

Filter Inversion

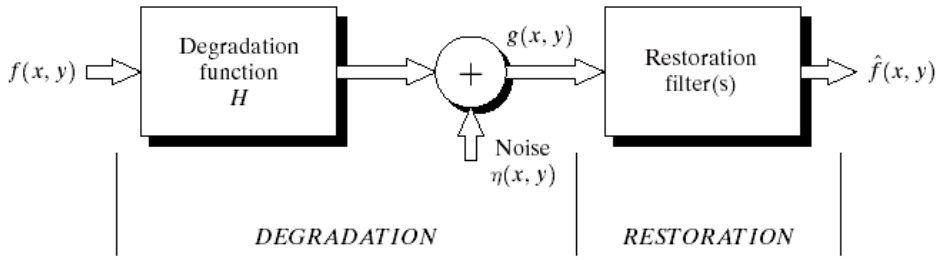

FIGURE 5.1 A model of the image degradation/restoration process.

$$g(x,y)=f(x,y)*h(x,y)+n(x,y) \qquad G(u,v)=F(u,v)H(u,v)+N(u,v)$$

$$\hat{F}(u,v)=\frac{G(u,v)}{H(u,v)}=F(u,v)+\frac{N(u,v)}{H(u,v)}$$

Inverse filter

Weiner filter

$$e^2=E\left\{(f-\hat{f})^2\right\}$$

$$\hat{F}(u,v)=\left[\frac{1}{H(u,v)}\frac{|H(u,v)|^2}{|H(u,v)|^2+\frac{|N(u,v)|^2}{|F(u,v)|^2}}\right]G(u,v)$$

Filter Inversion

a b
c d

FIGURE 5.27 Restoring Fig. 5.25(b) with Eq. (5.7-1). (a) Result of using the full filter. (b) Result with H cut off outside a radius of 40; (c) outside a radius of 70; and (d) outside a radius of 85.

Filter Inversion

a b c

FIGURE 5.28 Comparison of inverse- and Wiener filtering. (a) Result of full inverse filtering of Fig. 5.25(b). (b) Radially limited inverse filter result. (c) Wiener filter result.

Filter Inversion

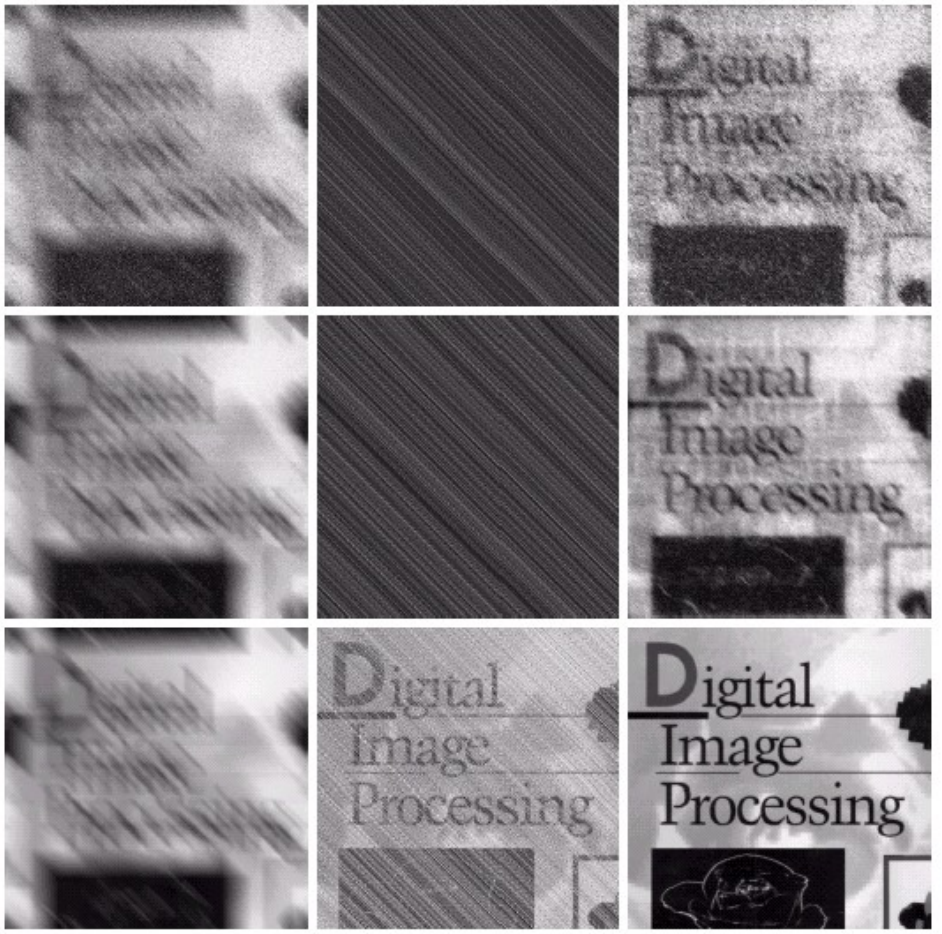

a b c
d e f
g h i

FIGURE 5.29 (a) Image corrupted by motion blur and additive noise. (b) Result of inverse filtering. (c) Result of Wiener filtering. (d)–(f) Same sequence, but with noise variance one order of magnitude less. (g)–(i) Same sequence, but noise variance reduced by five orders of magnitude from (a). Note in (h) how the deblurred image is quite visible through a "curtain" of noise.

Constrained Least Squares

$$\hat{F}(u,v)=\left[\frac{1}{H(u,v)}\frac{|H(u,v)|^2}{|H(u,v)|^2+\frac{|N(u,v)|^2}{|F(u,v)|^2}}\right]G(u,v)$$

Weiner

$$\frac{|N(u,v)|^2}{|F(u,v)|^2}=K$$

Constrained Least Square

$$\frac{|N(u,v)|^2}{|F(u,v)|^2}=\gamma|P(u,v)|^2$$

$$p(x,y)=\begin{bmatrix}0 & -1 & 0\\ -1 & 4 & -1\\ 0 & -1 & 0\end{bmatrix}$$

$$\|g-H*\hat{f}_\gamma\|^2=\|n\|^2$$

$$\|n\|^2=MN\left(\sigma^2+\mu^2\right)$$

Constrained Least Squares

a b c

FIGURE 5.30 Results of constrained least squares filtering. Compare (a), (b), and (c) with the Wiener filtering results in Figs. 5.29(c), (f), and (i), respectively.

UNIVERSITÀ
CA' FOSCARI
VENEZIA